

Article

Sustainable Option for Hydrogen Production: Mechanistic Study of the Interaction between Cobalt Pincer Complexes and Ammonia Borane

Yan Li ¹, Chi-Wing Tsang ^{2,*} , Eve Man Hin Chan ³, Eugene Yin Cheung Wong ⁴, Danny Chi Kuen Ho ⁴, Xiao-Ying Lu ² and Changhai Liang ^{5,*}

¹ School of Chemical Engineering, University of Science and Technology Liaoning, Anshan 114051, China; yanli@ustl.edu.cn

² Faculty of Science and Technology, Technological and Higher Education Institute of Hong Kong (THEi), Hong Kong 999077, China; xylu@vtc.edu.hk

³ Faculty of Design and Environment, Technological and Higher Education Institute of Hong Kong (THEi), Hong Kong 999077, China; evechan@vtc.edu.hk

⁴ Department of Supply Chain and Information Management, The Hang Seng University of Hong Kong, Hong Kong 999077, China; eugenewong@hsu.edu.hk (E.Y.C.W.); dannyho@hsu.edu.hk (D.C.K.H.)

⁵ Laboratory of Advanced Materials and Catalytic Engineering, School of Chemical Engineering, Dalian University of Technology, Dalian 116024, China

* Correspondence: ctsang@vtc.edu.hk (C.-W.T.); changhai@dlut.edu.cn (C.L.)

Received: 4 June 2020; Accepted: 26 June 2020; Published: 28 June 2020



Abstract: The mechanism of the solvolysis/hydrolysis of ammonia borane by iridium (Ir), cobalt (Co), iron (Fe) and ruthenium (Ru) complexes with various PNP ligands has been revisited using density functional theory (DFT). The approach of ammonia borane (NH_3BH_3) to the metal center has been tested on three different possible mechanisms, namely, the stepwise, concerted and proton transfer mechanism. It was found that the theoretical analyses correlate with the experimental results very well, with the activities of the iridium complexes with different PNP ligands following the order: $(\text{tBu})_2\text{P} > (\text{iPr})_2\text{P} > (\text{Ph})_2\text{P}$ through the concerted mechanism. The reaction barriers of the rate-determining steps for the dehydrogenation of ammonia borane catalyzed by the active species $[(\text{tBu})_2\text{PNP-IrH}]$ (Complex I-8), are found to be 19.3 kcal/mol (stepwise), 15.2 kcal/mol (concerted) and 26.8 kcal/mol (proton transfer), respectively. Thus, the concerted mechanism is the more kinetically favorable pathway. It is interesting to find that stable $(\text{tBu})_2\text{PNP Co-H}_2\text{O}$ and $(\text{tBu})_2\text{PNP Co-NH}_3$ chelation products exist, which could stabilize the active I-8 species during the hydrolysis reaction cycle. The use of more sterically hindered and electron-donating PNP ligands such as (adamantyl)₂P provides similar activity as the t-butyl analogue. This research provides insights into the design of efficient cobalt catalysts instead of using precious and noble metal, which could benefit the development of a more sustainable hydrogen economy.

Keywords: iridium PNP complexes; cobalt PNP complexes; ammonia borane hydrolysis; density functional theory; hydrogen production

1. Introduction

On-demand hydrogen production from stable chemical hydrides has been the subject of hydrogen energy research, as it ensures a safe and sustainable way for the development of hydrogen and fuel-cell based economy. Ever since the launch of the Hydrogen Fuel Initiative in 2004 by the US government, the hydrogen infrastructure and fuel cell technologies has been put on an accelerated schedule. Various aspects of research related to hydrogen have been advancing, including the production and

delivery of hydrogen, hydrogen storage and release, fuel cell technologies, hydrogen safety, etc. The US Department of Energy has just announced a new investment in funding research specifically in the (a) development of non-platinum catalyst in fuel cell; (b) advanced water splitting materials and technology and (c) unsolved challenges in the development of solid H₂ storage materials [1]. Over the past few decades, numerous research studies have been conducted, searching for the most effective H₂ storage materials and their H₂ release methods. Among the many H₂ solid storage materials, namely, MOF-5 adsorbent [2], BN-methyl cyclopentane [3], and complex hydride NaAlH₄ [4], ammonia-borane (AB) remains as the most promising solid H₂ storage materials, due to the high gravimetric hydrogen density of 19.6 wt%, low molecular mass, modest stability under ambient conditions and therefore suitable for both light-weight transportation and stationary applications [5,6]. Numerous new and high-performing molecular homogeneous catalysts with good stability and recyclability for releasing H₂ from ammonia-borane have been reported, and these technologies have been the focus of a number of reviews [7–11]. Two critical issues, which are yet to be solved, are determining whether such a catalytic technology could be part of the “hydrogen economy” in the near future, namely, (1) stable and highly efficient catalysts which are capable of releasing H₂ from ammonia-borane quantitatively with excellent recyclability and (2) the facile and economic way of the whole hydrogen production process, including both the cost of catalyst and the on-site regeneration of spent ammonia-borane [12]. In terms of stability and selectivity, homogeneous catalysts are more attractive than the heterogeneous counterparts due to their potential of exhibiting high selectivity through the design of intimate substrate-metal interactions, which could allow for controllable and reversible processes [13].

Iridium-based homogeneous catalysts are particularly efficient in releasing H₂ from ammonia-borane. Since the discovery of ammonia-borane dehydrogenation using iridium PCP pincer complexes by Goldberg et al. (1) [14], and the solvolysis of ammonia-borane using the air- and moisture- stable iridium PNP pincer complexes by Graham et al. (2) [15], several efficient iridium complexes have been reported, which are [IrH₂(η²-H₂)₂(PCy₃)₂]⁺ (3) [16,17], the [IrH₂(t^tBu)₂]⁺ [t^tBu = 1,3-bis(tert-butyl)imidazol-2-ylidene] (4) [18,19], the NHC-based Ir(IMes)₂H₂Cl (5) [20], the [Cp*Ir(6,6'-(OH)₂-bpy)(OH₂)]²⁺ (6) [21], [Ir(dppm)₂]⁺ (7) [22] and the IrHCl[(PPh₂(*o*-C₆H₄CO))₂H] (8) [23], as shown in Figure 1. Among these, catalysts (2), (4), (6) and (8) are extremely air- and moisture- stable and are capable of releasing three, or almost three, equivalents of H₂ from ammonia-borane, under solvolytic and hydrolytic conditions.

On the other hand, being the close analogue of Ir complexes, Co complexes are becoming increasingly important on base metal catalysis development, since they are more sustainable, cheap (Co: € 26.6/kg [24] Vs Ir: € 52,750/kg [25]) and non-toxic. Numerous cobalt catalysts, especially those complexes with PNP pincer, PCP pincer and PBP pincer ligands, have been found to be highly efficient towards olefin hydrogenation [26], carbon dioxide hydrogenation [27], olefin transfer hydrogenation [28], etc. The unique activity of these systems is due to the π-interaction between the cobalt metal and the donor atoms N and B. Nonetheless, the reports on the efficient dehydrogenation of ammonia borane under solvolytic/hydrolytic conditions using homogeneous Co-PNP catalysts are very rare, giving the relatively large amount of heterogeneous Co catalysts towards ammonia borane hydrolysis reaction [29]. Above all, the global warming potential of Co from cradle to gate is estimated to be ca. 8.3 kg CO₂-eq/kg, as compared with 8860 kg CO₂-eq/kg for Ir metal [30]. The search for Co catalysts with comparable activity similar to those of Ir is thus a vital need for the development of a more sustainable hydrogen economy.

It is interesting to note that catalyst (2) catalyzed a much faster hydrogen release process but with much slower release rate under normal water- and air-free catalytic dehydrogenation condition. While it has been proven that for (4), one equivalent of H₂ is from the water solvent and the Ir-NH₃ adduct is involved in the mechanism, the mechanism for the solvolysis of ammonia-borane by (2) remains elusive. Unlike t-butyl group of catalyst (4) and the hydroxyl group of catalyst (6), the t-butyl group of (2) remains intact, and oxidative addition was not involved during the hydrogen release mechanism. In addition, ammonia molecules were detected in the ammonia borane hydrolysis by catalyst (2) [15], and it was unclear whether this will have a promoting or detrimental effect to the

stability of the catalyst. This paper aims at elucidating this mechanism to complete the picture for the family of organometallic Ir complexes and exploring the possibility of further improving the catalytic activity of PNP-based catalysts for future hydrogen release applications.

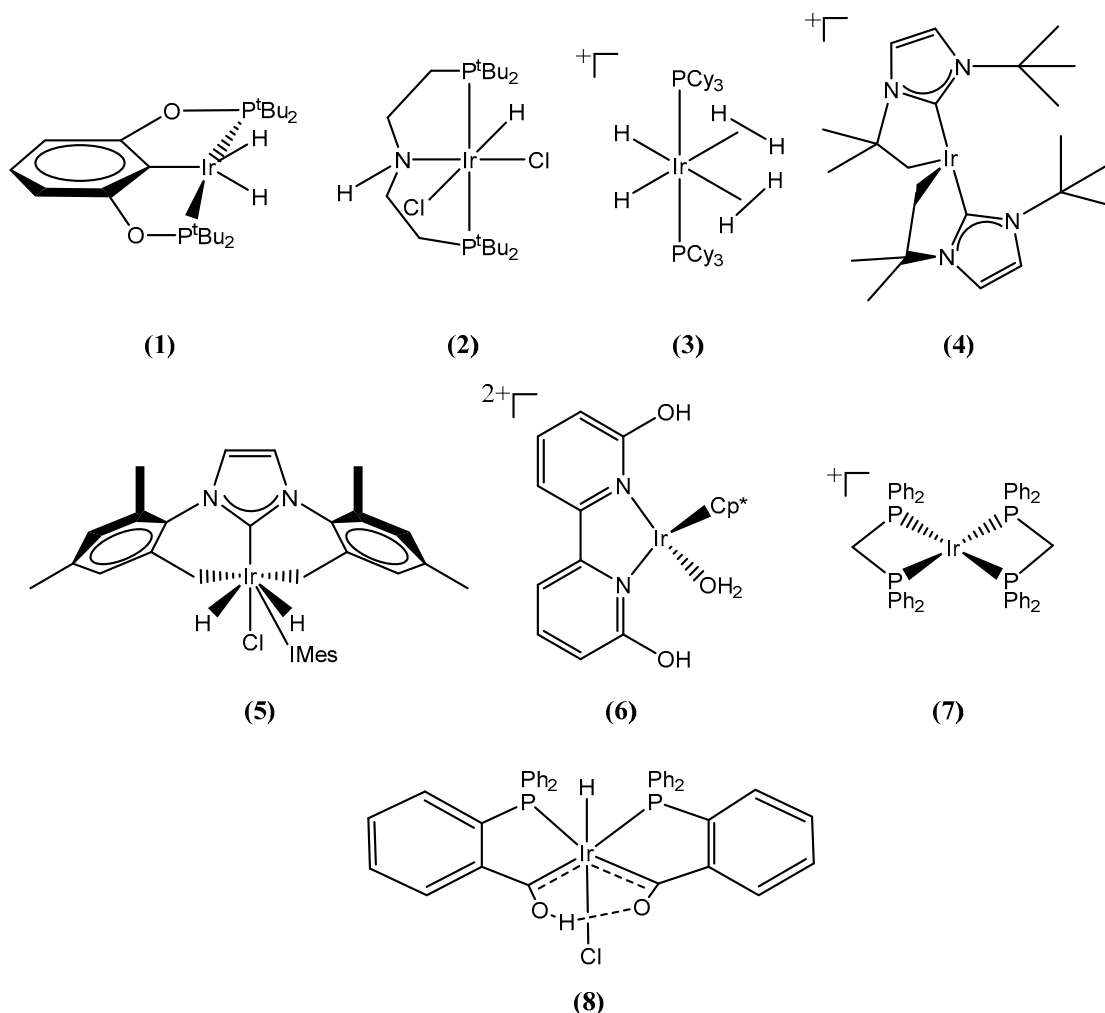


Figure 1. Various homogeneous iridium catalysts that are capable of releasing H_2 from ammonia borane: (1) η^3 -1,3-(OP^tBu_2) $_2C_6H_3$, (2) $NH[(CH_2)_2P^tBu_2]_2IrCl_2H$, (3) $[IrH_2(\eta^2-H_2)_2(PCy_3)_2]^+$, (4) $[IrH_2(I^tBu)_2]^+$ [I^tBu = 1,3-bis(tert-butyl)imidazol-2-ylidene], (5) $Ir(IMes)_2H_2Cl$, (6) $[Cp^*Ir(6,6'-(OH)_2-bpy)(OH_2)]^{2+}$, (7) $[Ir(dppm)_2]^+$, (8) $IrHCl[(PPh_2(o-C_6H_4CO))_2H]$.

2. Results and Discussion

Effective and efficient homogeneous catalysts for the catalytic dehydrogenation of ammonia borane and their applications in hydrogen release reactions have been extensively studied and reviewed [7,11]. The first efficient dehydrogenation of ammonia borane was reported by Goldberg on using a type of pincer iridium POCOP complex (1) [η^3 -1,3-(OP^tBu_2) $_2C_6H_3$] [14]. Maximally one equivalent of H_2 was produced per monomer, and an oligomeric B-N byproduct was observed and was proved to be a cyclic pentamer (NH_2-BH_2) $_5$ [31]. It was also found that a resting piece (POCOP)IrH(η^2 -BH $_4$) (9) (Figure 2) was responsible for preventing the further activation of the ammonia borane molecule. Such a phenomenon was also observed for the Rh complex by excess BH $_3$ poisoning, leading to the ceasing of the dehydro-coupling of dimethyl ammonia borane [14]. Concerted H $^+$ and H $^-$ removal from the ammonia borane monomer was suggested through the boron end hydrogen atom [32]. A similar mechanism was observed for the bis-phosphine complex (10) [17] and (11) (Figure 2) [20], in which methyl ammonia borane and dimethyl ammonia borane

were observed to coordinate to the iridium centers through the bis-hydride/alkyl tethered manners. Oligomerization was also observed when ammonia borane and methyl ammonia borane were used. However, with bis-diphosphine ligand dppm, complex (7) underwent an oxidative addition mechanism to form the complex $[\text{Ir}(\text{H})(\text{BH}_2\cdot\text{NH}_3)(\text{dppm})_2]^+$, followed by the release of one equivalent of H_2 . Thus, the dehydrogenation of ammonia borane by homogeneous iridium catalysts was quite catalyst- and substrate-specific.

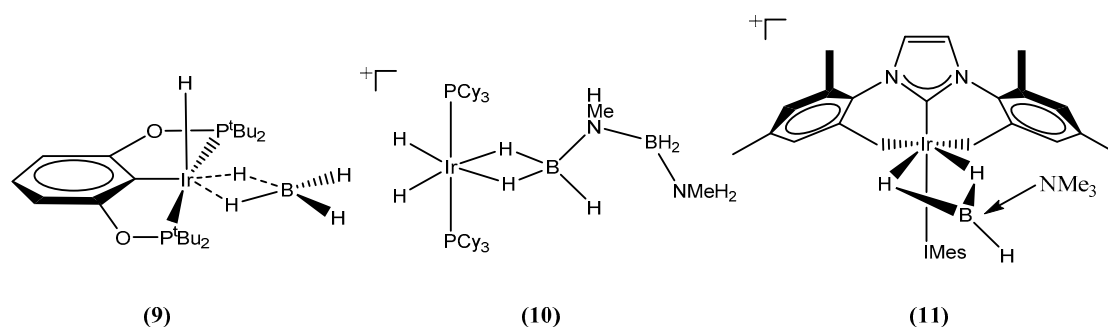
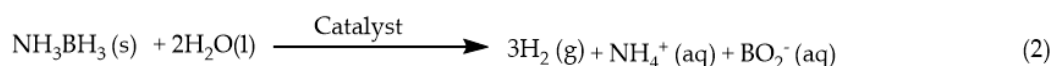
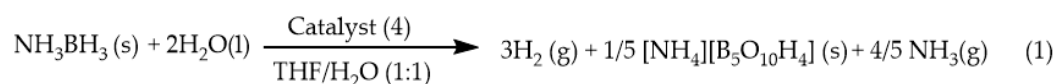


Figure 2. Intermediates detected during the dehydrocoupling of ammonia borane by catalyst (1), (3) and (5) respectively.

Under solvolytic or hydrolytic conditions, the mechanism of ammonia borane activation can be totally different and may involve the coordination of small molecules, such as NH_3 and H_2O , to the metal centers. Almost at the same time, three very robust and active catalysts, (2) [15], (4) [18] and (8) [33], were found to release three, or almost three, equivalents of H_2 within 30 mins, with excellent recyclability. The H_2 release mechanism of (4) was first proposed by Nolan et al., through the Ir-mediated cleavage of the B–N bond of the ammonia borane. Two cationic Ir– NH_3 complexes had been isolated and were proposed to be resting states of the active catalyst. The bis-ortho–metalated catalyst shows rapid and quantitative evolution of hydrogen from ammonia borane at room temperature. It was later suggested by Wong et al. that the activation of ammonia borane actually proceeded through the proton transfer pathway, which is kinetically most favorable among other proposed pathways. Thus, it is quite different from the concerted B–H/N–H bond activation mechanism for catalyst (1). Under base addition such as methylamine and aromatic amine, amine-iridium adducts were found for complex (8) under solvolytic/hydrolytic conditions [33,34]. Moreover, the reactions between the catalyst and the ammonia-borane were always found to generate ammonia gas [18,35]. According to equation (1), one possible borate product was suggested, concomitant with the release of 4/5 ammonia molecule. NH_3 (g) may then have interacted with the catalyst, as shown in Scheme 1. If NH_3 molecules were not observed in the hydrolysis of ammonia borane, in general, equation (2) follows [36]. In this study, we aimed to investigate the mechanism of the hydrolysis of ammonia borane using (2) on the base effect, metal effect, ligand effect, and finally, the adduct effect.



Scheme 1. Different fate of ammonia borane hydrolysis.

2.1. When Base is Involved in the Reaction Mechanism—Formation of Cationic Iridium Species

Experimentally, the catalytic release of H_2 by (2) can be facilitated, both with and without base [37,38]. As shown in Figure 3, two possible geometries can be found after the extraction of the

chloride ion with sodium *t*-butoxide, i.e., complex I-Cat A and complex I-Cat B cations. The ammonia borane molecule then approaches to the cationic iridium metal center through a stepwise mechanism through the hydridic hydrogen on boron. To simplify the calculation, we first use PH₂ as the phosphine ligand model. Using the B3LYP calculation method, the reaction energy barrier of Pathway I-A and I-B is determined to be 47.0 kcal/mol (Figure 4) and 31.6 kcal/mol (Figure 5) respectively. Thus, under the experimental conditions, pathway I-B and the respective geometry are most likely to occur.

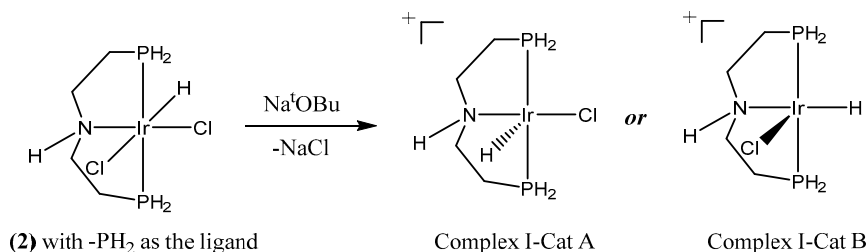
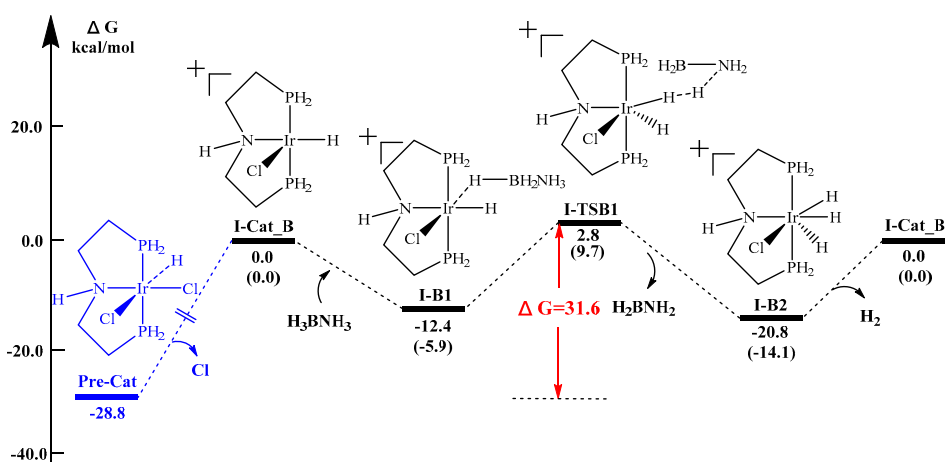
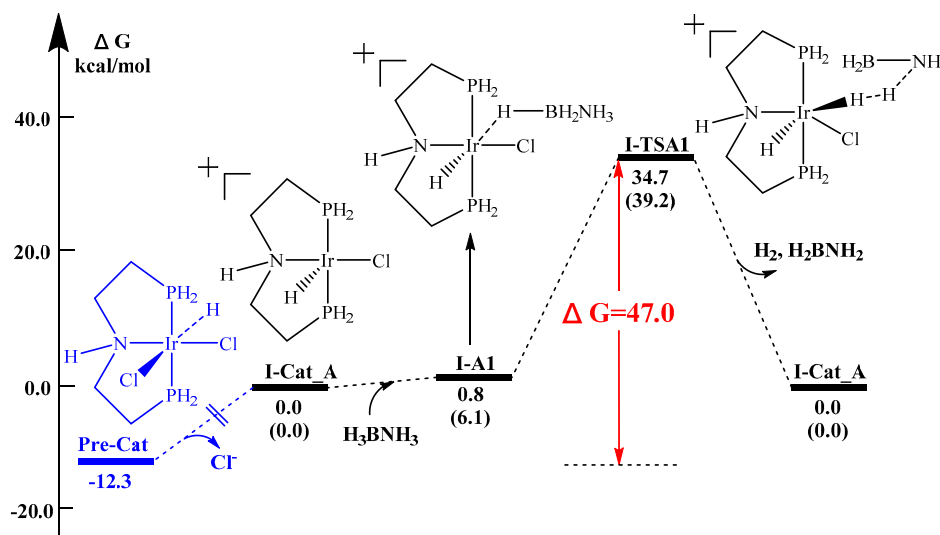


Figure 3. Possible geometries of the products from the reaction of catalyst precursor (2) with strong base.



Metal Effects

When the substituent on the phosphine of the PNP ligand is ^tBu group, the optimal path with different metals participating in the reaction is calculated (as shown in Figure S2). It can be estimated that when the metals are Ir, Ru and Co, the reaction energy barriers are 21.5, 31.5 and 37.4 kcal/mol, based on the B3LYP geometry, respectively. So, the calculated reaction order is Ir > Ru > Co, which is in accordance with the experimental results reported earlier [37,38]. The solvent effects and effects of different PNP ligands for the cationic species were also performed using M06 method, and the results were shown on P.5 in the Supplementary Materials for comparison (Figure S3a,b). The highest activity with using PNP ligands with P(^tBu) group was also in close agreement with the experiment studies.

2.2. When Base is Not Involved in the Reaction Mechanism—Neutral Iridium Species

Since B3LYP was proved to be a suitable modeling method, we have extended the method to the comprehensive studies of neutral iridium species, where a base is not involved. When a base is not used in the reaction, the H₂ release mechanism may follow the reaction scheme, as shown in Figure 6. This is proposed according to a similar reaction between the pre-catalyst [Ru(p-Cym)(bipy)Cl]Cl and excess ammonia borane in H₂O/THF mixed solvent system [39]. In addition, the existence of structure of the catalyst (2)—monohydride dichloride [15] and monochloride dihydride—has been unequivocally proven by X-ray crystallography and spectroscopic data [37,38]. According to the literature, we attempt to investigate the three most plausible mechanism for the H₂ release mechanism by complex I-8, without the addition of a base.

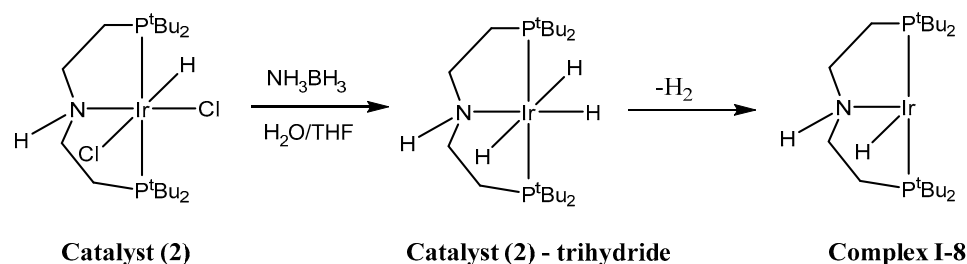


Figure 6. Formation of the coordinatively unsaturated complex I-8 which is capable of releasing H₂ from ammonia borane.

2.2.1. Stepwise Mechanism (Path 1)

To simplify the structural optimization, a total of four pathways with different geometries for the stepwise B-H and N-H activation of the dehydrogenation of ammonia borane have been found computationally, in which the most feasible one was shown in Path 1a (blue path, Figure 7). All the intermediates and transition states species are fully optimized at the B3LYP/6-31G** (LANL2DZ) level. Ammonia borane first coordinated to complex I-8 through a B-H-Ir single bridge, to form the σ -complex 9-1a, which is higher than complex I-8 in energy by 3.3 kcal/mol. Further B-H activation (TS9-1a), followed by the formation of the Ir-H bond, led to the formation of complex 10-1a. Subsequent N-H activation led to the transition state TS10-1a, in which it has the highest barrier and could be the rate-determining step for stepwise mechanism. After the transition state TS10-1a, NH₂BH₂ was released, and finally, the catalyst was regenerated through the release of H₂ from TS11, with an activation barrier of 32.4 kcal/mol and the catalytic cycle completed. The H₂ release barrier was considered to be much higher than the reported value for the [Ir(^tBu')₂]⁺ catalyst complex (2.39 kcal/mol) [19]. The transition states involved in this path are TS9-1a (7.0 kcal/mol, relative to complex I-8) and TS10-1a (8.8 kcal/mol, relative to complex I-8). The remaining three other pathways with different geometries were presented in the supporting materials for reference (Figure S4).

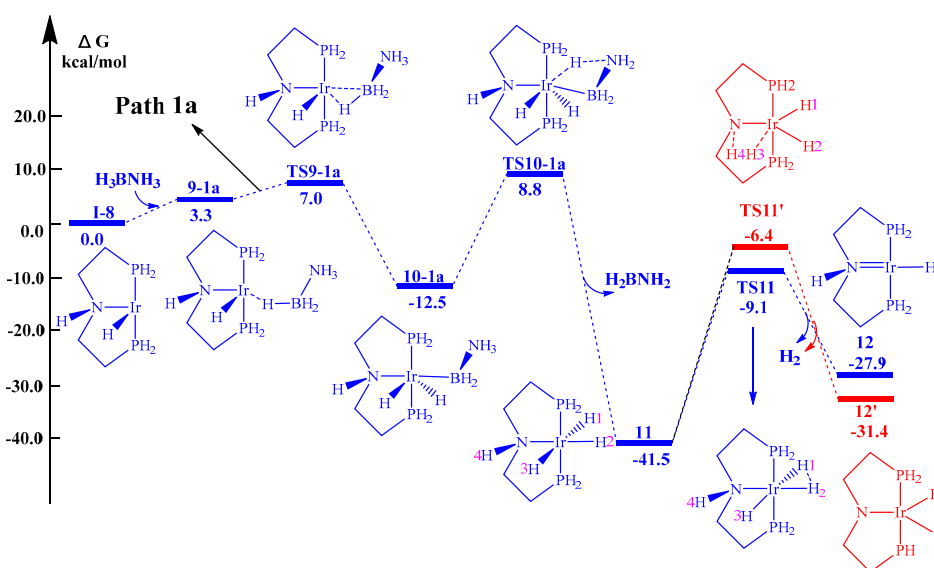


Figure 7. Stepwise reaction potential surface starting from intermediate I-8.

2.2.2. Concerted Mechanism (Path 2)

A total of only two pathways with different geometries were found computationally for concerted B-H/N-H activation. In contrast to the reported literature [19], it was found that the concerted B-H/N-H activation could begin with both the σ -complex formed by both N-H-Ir (9-2a) and B-H-Ir (9-2b) bridges. Afterwards, the proton from both the B and N atoms transfer to the iridium center in a concerted manner, to form the iridium trihydride complex 11. Comparing the energy barriers, the activation barrier for TS9-1a is somewhere between those for TS9-2a and TS9-2b, where the N-H activation pathway leading to the intermediate TS9-2a is the most feasible pathway, i.e. 5.2 kcal/mol. The pathway Path 2a via the transition state TS9-2a (5.2 kcal/mol) is thus found to be the most feasible, as shown in Figure 8. For the five member ring transition state complex TS9-2a, the B-H, N-H, Ir-H(B) and Ir-H(N) interatomic distances are found to be 1.339 Å, 1.343 Å, 1.839 Å and 1.775 Å, respectively (imaginary frequency = 999i), which were shorter than those reported values [19]. This is because the ligand and the electric charge of the transition states are both different from the literature model, leading to the difference in the bond length. The TS11 of both the stepwise and concerted mechanism have the same activation barriers.

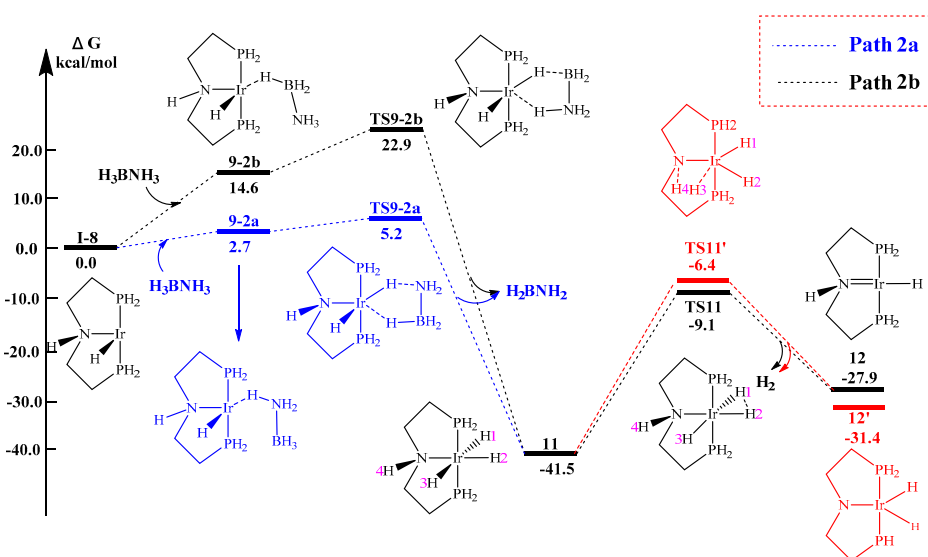


Figure 8. Concerted reaction potential surface starting from intermediate.

2.2.3. Proton Transfer Mechanism

Regarding the calculations previously reported [19], we have designed a new path (as shown in Figure S5) for the proton transfer pathway. In this model, ammonia borane first coordinated to complex I-8 through the boron atom, followed by the migration of B-H to iridium to form a three-member ring transition state. Another possibility is that the ammonia borane can also coordinate to complex I-8 through the nitrogen atom, followed by the migration of N-H to iridium, however, this leads to a four-member ring transition state which could have even high energy barrier than the B-H-Ir transition state. The energy of the transition state involved in the process is rather high (TS9-3, 89.0 kcal/mol), rendering this pathway less feasible. The extreme high energy barrier of TS9-3 is probably due to the steric strain exerted by the Ir-B-H three-member ring. The reaction barrier of the specific transition states based on both a simplified (H_2P -) and complete model ($^t\text{Bu}_2\text{P}$ -) are listed in Table 1 for comparison.

Table 1. Summary of the reaction energy barrier of the rate-determining steps of Path 1a, Path 2a, Path 2b and Path 3, based on simplified and complete model (kcal/mol).

	Path 1a 10-1a → TS10-1a	Path 2a I-8 → TS9-2a	Path 2b I-8 → TS9-2b	Path 3 I-8 → TS9-3
Simplified model (H_2P -)	21.3	5.2	22.9	38.6
Complete model ($^t\text{Bu}_2\text{P}$ -)	19.3	15.2	34.5	26.8

Comparing the energy of the transition states involved in the above three mechanisms, the concerted mechanism is the most probable pathway. For the most feasible pathway—Path 2a, we have tested the effect of substituents and different metals, in an attempt to get the full picture of the energy level distributions.

2.2.4. Metal Effects

The test results for different metal centers for the most feasible path ($\text{I-8} \rightarrow \mathbf{9-2a} \rightarrow \text{TS9-2a} \rightarrow \mathbf{11} \rightarrow \text{TS11}(\text{TS}(\mathbf{11}')) \rightarrow \mathbf{12}(\mathbf{12}')$), i.e. the concerted mechanism, were computationally investigated. Using the complete model ($^t\text{Bu}_2\text{P}$ -), the most feasible pathway with the catalyst having the Co, Fe and Ru centers were tested and were compared to Ir. In order to make the figure clearer, the energy profile from $\text{I-8} \rightarrow \mathbf{9-2a} \rightarrow \text{TS9-2a} \rightarrow \mathbf{11} \rightarrow \text{TS11} \rightarrow \mathbf{12}$ was shown in Figure S6a, while from $\text{I-8} \rightarrow \mathbf{9-2a} \rightarrow \text{TS9-2a} \rightarrow \mathbf{11} \rightarrow \text{TS11}' \rightarrow \mathbf{12}'$, the reaction energy profile was given in Figure S6b. It can be seen from the potential energy map that:

- (1) except for the Ir center, the $\mathbf{11} \rightarrow \text{TS11}' \rightarrow \mathbf{12}'$ pathways for all the other metal centers have lower activation barriers than the $\mathbf{11} \rightarrow \text{TS11} \rightarrow \mathbf{12}$ pathway;
- (2) in Figure S6a, for the reaction of the first step ($\text{I-8} \rightarrow \text{TS9-2a}$) and the second step ($\mathbf{11} \rightarrow \text{TS11}$), the energy barriers are calculated as follows: the energy barrier of Ir is 15.2 and 30.5 kcal/mol; the energy barrier of Co is 18.2 and 12.6 kcal/mol; the energy barrier of Fe is 44.7 and 1.8 kcal/mol; the energy barrier of Ru is 43.7 and 2.4 kcal/mol. The order of energy barrier is $\text{Co} < \text{Ir} < \text{Fe} < \text{Ru}$, so the reaction rate is $\text{Co} > \text{Ir} > \text{Fe} > \text{Ru}$;
- (3) in Figure S6b, for the reaction of the first step ($\mathbf{8} \rightarrow \text{TS9-2a}$) and the second step ($\mathbf{11}' \rightarrow \text{TS11}'$), the energy barriers are calculated as follows: the energy barrier of Ir is 15.2 and 28.6 kcal/mol; the energy barrier of Co is 18.2 and 21.0 kcal/mol; the energy barrier of Fe is 44.7 and 19.6 kcal/mol; and the energy barrier of Ru energy barrier is 43.7 and 25.4 kcal/mol. The order of energy barrier is $\text{Co} < \text{Ir} < \text{Fe} < \text{Ru}$, so the reaction rate is $\text{Co} > \text{Ir} > \text{Fe} > \text{Ru}$. It contradicts with the experimental results that the Co complex with $^t\text{Bu}_2\text{P}$ -substituents did have lower reactivity towards ammonia borane; this can be explained by the finding of a much lower water molecules chelated Co-I-8 complex as a resting form (vide infra Section 2.2.6).

At the final stage of the reaction, the intermediate 11 evolving hydrogen to form 12 has two different possible outcomes. The difference lies between the structure of the intermediate 12 and the

structure of the intermediate **12'**, mainly at the position of H attachment to the metal. The transition state of this process is TS11 (32.4 kcal/mol), as shown in Figure S7.

2.2.5. Ligand Effects

In our observed experiment, PNP-Ir pincer complex with ^tBu₂P- substituent is more reactive than the ⁱPr₂P- analogue. This may be due to the instability of ⁱPr-PNP-Ir complexes under solvolytic or hydrolytic conditions, such as a metal leaching problem, instead of PNP ligand effects (both electronic and steric effects). Thus, the four ligands with different phosphine substituents, ^tBu, Me, Ph and ⁱPr, were computationally investigated for the complete model structure (geometric optimization and single point energy) of all species from intermediates **I-8** to **12**. The results concluded that the ^tBu ligand works best. The energy barrier is significantly lower than the energy barrier among those of other ligands. As can be seen from the figures shown in the Supplementary Materials (Figure S8a–d, corresponding to the substituents ^tBu, Me, Ph and ⁱPr respectively), the energy barriers of TS11 transition states of the four ligands follow the order: 30.5 kcal/mol (^tBu) < 31.7 kcal/mol (Ph) < 32.0 kcal/mol (ⁱPr) < 35.5 kcal/mol (Me). For the TS11' transition state complexes, the order of the energy barriers of the four ligands are: 28.6 kcal/mol (^tBu) < 31.7 kcal/mol (ⁱPr) < 32.7 kcal/mol (Ph) < 34.5 kcal/mol (Me). It can be seen that the energy barrier of the ^tBu ligand is always lower than that of the other three ligands, regardless of the TS11 or TS11' states. Moreover, the reaction exergon of generating the **12'** state is 42.2 kcal/mol, which is much greater than the exergon of other ligands. In addition, the energy barrier of 28.6 kcal/mol indicated that the reaction can be completed under such very mild experimental conditions, i.e. 40 °C.

It is thus very interesting to know if more sterically hindered and electron donating phosphine substituents could have a significant impact on the activity of the iridium complexes. Similar computational test was thus performed for the PNP ligand with (adamantly)₂P- substituents. We have tested this hypothesis for the most feasible path **I-8** → **9-2a** → **TS9-2a** → **11** → **TS11 (TS(11'))** → **12(12')**, as shown in Figure S9, and the metal center being investigated is Ir. As can be seen, the rate determining step of the process is **11** → **TS11 (TS(11'))**, and the corresponding energy barrier is 30.0 and 29.1 kcal/mol respectively for the two different products, which is very close to the energy barrier of the ^tBu ligand (30.5 and 28.6 kcal/mol). In accordance with the experimental observed results, the PNP ligand with (adamantly)₂P- substituents of the Ir complexes does have similar experimental activity.

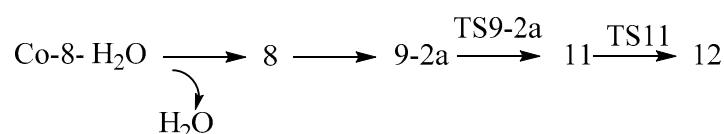
2.2.6. Effects of NH₃ and H₂O Adduct

Since a very small amount of NH₃(g) was liberated during the reaction [15], it would be interesting to know whether these small molecules could have either stabilization or detrimental effects to the metal center. As well, it was also observed that H₂O-iridium could be one resting form during the hydrolysis reaction [21]. Therefore, in this section, we aim to investigate the possibility of adduct formation for (2). Using the simplified model, i.e. with PH₂- as the ligand substituent, density functional theory (DFT) results showed that only one complex of NH₃ molecules can barely lower the energy barrier of Intermediate **I-8**; the corresponding stabilizers are 8-1nh3-1 and 8-1nh3-2, as shown in Table S2. Compared with Intermediate **I-8** (0.0 kcal/mol), 8-1nh3-1 (−1.7 kcal/mol) and 8-1nh3-2 (−1.0 kcal/mol) were reduced by 1.7 and 1.0 kcal/mol, respectively.

Thus, using the complete model ^tBu-PNP-Ir, the stabilization of structure **I-8** using the potential energy surface by small molecules H₂O, NH₃ and THF was investigated, as shown in Table S3a. In addition, Ir, Fe, Ru and Co metal centers were also investigated, where the results of Co were shown in Table 2. (The data for Fe and Ru were shown in Table S3b and Table S3c in Supplementary Materials, respectively). It can be seen, from Table S3a, that for the Ir center, none of the three small molecules can stabilize the intermediate structure **I-8**. It was also proven that the involvement of H₂O chelation does not favor the activation of NH₃BH₃ molecule, as shown in Figure S10 and Table S4. Interestingly, it was found that, for the Co center, although THF cannot stabilize the structure **I-8**, but H₂O and NH₃ can stabilize the structure **I-8**, namely, the Co-8-h2o-4 and the Co-8-nh3-4, so the system **8** mainly exists

in the form of Co-8-H₂O and Co-8-NH₃. Taking these species into consideration for the whole reaction process, the starting point became Co-8-H₂O or Co-8-NH₃. Thus, the entire reaction path, taking H₂O adduct as an example, is described in Scheme 2.

After taking the H₂O chelation into account, the total reaction energy barrier of the reaction pathway is 35.4 kcal/mol (Co-8-H₂O → TS9-2a), as shown in Figure 9. The energy barrier is significantly higher than the total reaction energy barrier when the reaction center is Ir (30.5 and 28.6 kcal/mol corresponds to the path of 12 and 12', respectively). This explained why Co is less reactive than Ir from the perspective of energy barrier. Because the experimental results are similar for the activity of the catalyst with ^tBu substituted phosphine ligand and substituted phosphine adamantyl ligand (Ada), in order to further verify that our conclusions also apply to adamantyl ligand, we tested small molecules H₂O, NH₃ and THF for the Co-adamantyl-PNP complex. The results of the stabilization effects were shown in Tables 3 and 4.



Scheme 2. Proposed reaction pathway for reaction between NH₃BH₃ and ^tBu-PNP-Co.

Table 2. The effect of H₂O, NH₃ and THF to the stabilization of complex I-8 (^tBu-PNP-Co).

Chelation	Species	Relative Energy (kcal/mol)
No chelation	Co-8	0.0
H ₂ O	Co-8-h2o-1	13.6
	Co-8-h2o-2	13.7
	Co-8-h2o-3	13.6
	Co-8-h2o-4	-17.5
	Co-8-h2o-5	12.7
	Co-8-h2o-6	13.3
NH ₃	Co-8-nh3-1	7.3
	Co-8-nh3-2	7.4
	Co-8-nh3-3	7.4
	Co-8-nh3-4	-17.2
	Co-8-nh3-5	7.1
	Co-8-nh3-6	7.1
THF	Co-8-thf-1	18.6
	Co-8-thf-2	17.5
	Co-8-thf-3	19.1
	Co-8-thf-4	8.3
	Co-8-thf-5	18.4
	Co-8-thf-6	18.4

Table 3. The effect of H₂O, NH₃ and THF to the stabilization of complex I-8 (Ada-PNP-Ir).

Chelation	Species	Relative Energy (kcal/mol)
	Ir-8	0.0
H ₂ O	Ir-8-h2o-1	18.8
	Ir-8-h2o-2	8.7
	Ir-8-h2o-3	7.4
	Ir-8-h2o-4	3.8
	Ir-8-h2o-5	8.1
	Ir-8-h2o-6	18.5

Table 3. Cont.

Chelation	Species	Relative Energy (kcal/mol)
NH ₃	Ir-8-nh3-1	13.0
	Ir-8-nh3-2	13.0
	Ir-8-nh3-3	11.8
	Ir-8-nh3-4	9.2
	Ir-8-nh3-5	12.0
	Ir-8-nh3-6	12.4
THF	Ir-8-thf-1	23.0
	Ir-8-thf-2	23.5
	Ir-8-thf-3	13.0
	Ir-8-thf-4	22.5
	Ir-8-thf-5	22.0

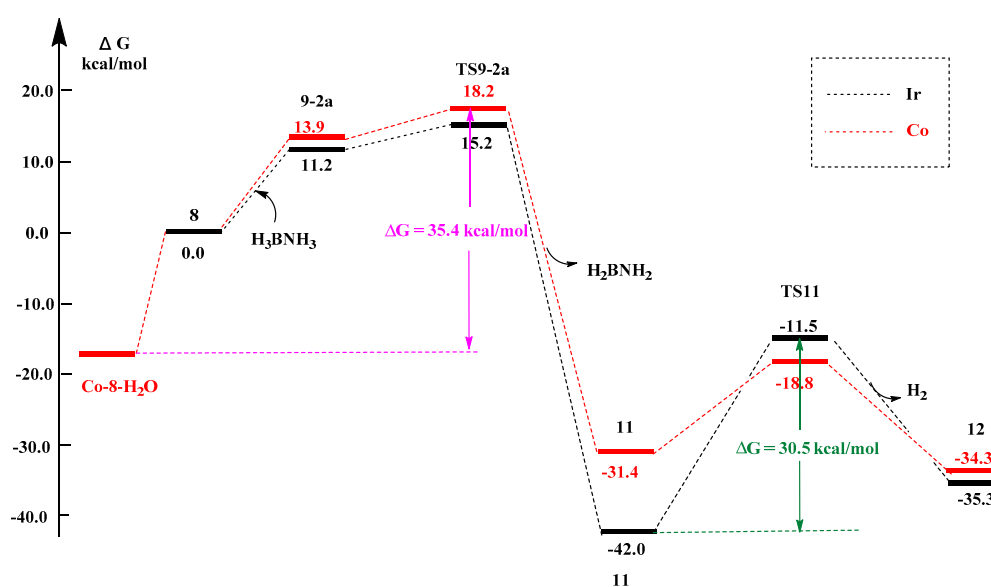


Figure 9. Potential energy profile for reaction between iridium/cobalt PNP complex with (^tBu)₂P-substituents and ammonia borane.

Table 4. The effect of H₂O, NH₃ and THF on the stabilization of complex I-8 (Ada-PNP-Co).

Chelation	Species	Relative Energy (kcal/mol)
H ₂ O	Co-8	0.0
	Co-8-h2o-1	15.5
	Co-8-h2o-2	14.3
	Co-8-h2o-3	13.8
	Co-8-h2o-4	-16.6
	Co-8-h2o-5	17.3
	Co-8-h2o-6	16.4
NH ₃	Co-8-nh3-1	8.6
	Co-8-nh3-2	8.4
	Co-8-nh3-3	-16.5
	Co-8-nh3-4	18.5
	Co-8-nh3-5	9.0
THF	Co-8-thf-1	19.3
	Co-8-thf-2	19.3
	Co-8-thf-3	11.1
	Co-8-thf-4	11.7
	Co-8-thf-5	19.9

It can be seen from Tables 3 and 4 that the three small molecules cannot stabilize the Ir-adamantyl-PNP; however, H₂O and NH₃ can stabilize the adamantyl-PNP-Co (relative energy of -16.6 kcal/mol for H₂O and -16.5 kcal/mol for NH₃) at the I-8 stage. Thus, it is expected that if the adamantyl-PNP-Co(I) complex could be synthesized, it would be more stable than adamantyl-PNP-Ir towards the solvolysis of ammonia borane, as shown in Figure 10. Yet, the reactivity of these two species need to be investigated and compared experimentally, in order to confirm these computational results.

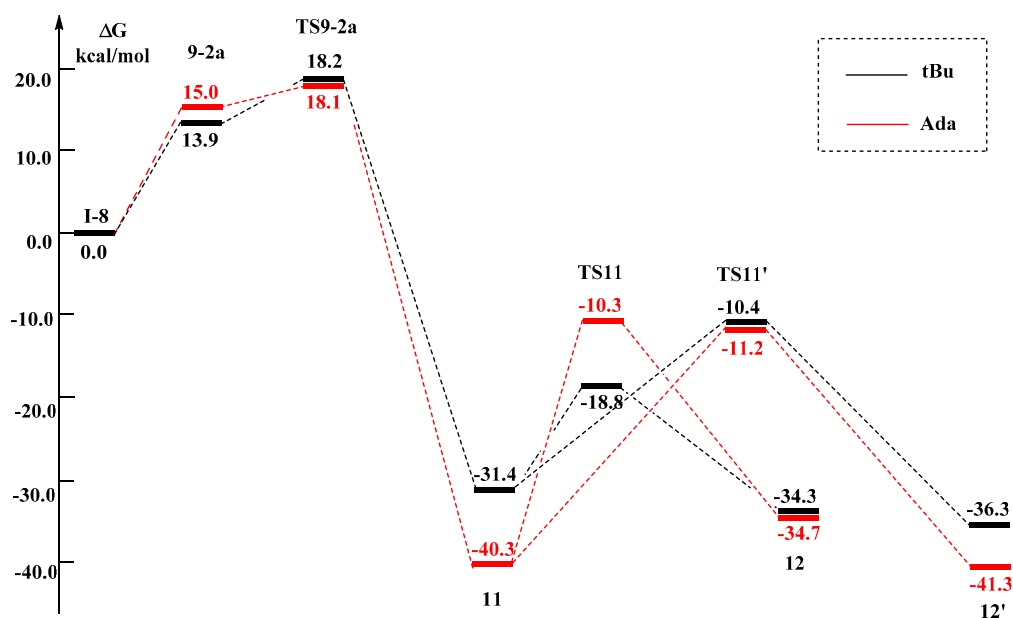


Figure 10. Potential energy profile for reaction between cobalt PNP complex with (tBu)₂P- and (adamantly)₂P- substituents and ammonia borane.

3. Materials and Methods

All the density functional theory (DFT) calculations were performed with the Gaussian 09 software package (Gaussian 09 (Revision D.01), Gaussian, Inc.; Wallingford, CT, USA, 2013) [40]. Geometries of all the stationary points, such as reactants, intermediates, transition states and products, were optimized using the B3LYP method [41,42]. To verify that our chosen computational method is reliable, other functionals and basis sets, such as method M06/TZVP, were also used to optimize the geometry of the pre-cat species. It was found that the theoretical values do not differ much from the experimental values [15]. (For a comparison of the results by various methods using B3LYP and M06, please refer to Figure S1 and Table S1 in the Supporting Materials). Note: the M06 [43] calculations were used to calculate the most energy favorable pathway for the cationic Ir species involved (i.e., Pathway I-B Figure S3(a) and S3(b) for the cationic Ir species), since the results using the B3LYP method were not consistent with the experimental results. In DFT computations, the LanL2DZ [44] basis set, including a double- ζ valence basis set with the Hay and Wadt effective core potential, was used to describe Ir, Co, Re, Ru, Fe. The 6-31G (d,p) basis set was used for all other atoms. Frequency calculations were performed, in order to verify that (1) all minima have zero imaginary frequency and (2) all transition states have only one imaginary frequency, as well as to obtain thermodynamic corrections at 313.15 K and 1 atm. Intrinsic reaction coordinate (IRC) calculations [45,46] were carried out to confirm that the transition states indeed connect two relevant minima. The solvent effects of THF and water were considered by performing single point energy calculations for the optimized structures using the SMD solvation model [47]. Single point energy calculations were carried out for the B3LYP and M06 (only for Pathway I-B, Figure S3a,b) levels, together with a larger basis set, in which the basis set for metal centers were kept unchanged and that for the other atoms were enlarged to 6-311++G (d,p).

The methodology is similar to other research groups to calculate single point energies in the solvent phase modeled by the solvation model SMD, using the gas phase optimized structures for reactions between organic substrates and organometallic catalysts [48–54].

4. Conclusions

The mechanism of the hydrolytic dehydrogenation of ammonia borane (NH_3BH_3) by different homogeneous catalysts with different metal centers (both cationic Ir and neutral Ir species, Co, Fe, Ru) complexing with various PNP ligands have been elucidated on three different possible pathways, namely, the stepwise, concerted and proton transfer pathways. This process resembles the non-hydrolytic dehydrogenation of ammonia borane by the Ir pincer complex (1), but is different from the hydrolytic dehydrogenation of ammonia borane by Ir carbene complex (4) [32], where a proton transfer mechanism was adopted [19]. The theoretical analyses correlate with the experimental results very well, with the activities of the iridium complexes with different PNP ligands following the order: $(^t\text{Bu})_2\text{P} > (^i\text{Pr})_2\text{P} > (\text{Ph})_2\text{P}$, through the concerted mechanism, where the reaction barriers of the rate-determining steps catalyzed by the active species $[(^t\text{Bu})_2\text{PNP-IrH}]$ (Complex I-8) were found to be 15.2 kcal/mol. Interestingly, significantly higher reaction energy barriers were found for a Co- H_2O chelation species ($\Delta G = 35.4$ kcal/mol), which explained the lesser reactivity of Co pincer complexes towards ammonia borane hydrolysis from the perspective of the energy barrier. Nevertheless, the stabilized resting form of I-8-Co- H_2O could indicate a more stable catalyst which can exhibit better recyclability. Besides, the use of even more electron-donating and sterically hindered PNP ligands could provide hints toward the development of metal pincer complexes, with even better performance towards the hydrolytic dehydrogenation of ammonia borane.

Supplementary Materials: The following are available online at <http://www.mdpi.com/2073-4344/10/7/723/s1>, Figure S1: Optimized structures for the Pre-Cat, Figure S2: Reaction potential energy surface of Pathway I-B with different metal centers involved in the H_2 release reaction, Figure S3: (a) When the solvent is THF, the potential energy surface of Pathway I-B of using phosphine ligands with various substituents optimized at the M06 level; (b): The potential energy surface of Pathway I-B with different PNP ligands when the reaction was carried out in pure H_2O optimized at the M06 level, Figure S4: The other three pathway for the Stepwise Mechanism, Figure S5: Potential energy transfer surface of proton transfer reaction starting from intermediate 8, Figure S6: (a) ^tBu being the substituent, the potential energy surface corresponding to the intermediates $8 \rightarrow 12$; (b): ^tBu being the substituent, the potential energy surface corresponding to the intermediates $8 \rightarrow 12'$, Figure S7: Difference in the energy profile between intermediate complex 12 and complex 12', Figure S8: (a) The potential energy surface corresponding to the intermediates $8 \rightarrow 12(12')$ with ^tBu - being the phosphine substituent; (b): The potential energy surface corresponding to the intermediates $8 \rightarrow 12(12')$ with Me- being the phosphine substituent; (c): The potential energy surface corresponding to the intermediates $8 \rightarrow 12(12')$ with Ph- being the phosphine substituent; (d): The potential energy surface corresponding to the intermediates $8 \rightarrow 12(12')$ with ^iPr - being the phosphine substituent, Figure S9: Potential energy profile for reaction between iridium PNP complex with (adamantly) $_2\text{P}$ - substituents and ammonia borane, Figure S10: The energy profile (kcal/mol) of the NH_3BH_3 activation reaction with and without the chelation of H_2O to the Ir metal center, Table S1: Major bond lengths calculated at different calculation levels, and the last column is the experimental values, Table S2: Preliminary test on the chelation of NH_3 to intermediate I-8 (simplified PH_2P - model). For 8-Xnh3-Y, X denotes the number of NH_3 molecules; Y denotes the chelation of NH_3 at different orientation to the metal, Table S3: (a): The effect of H_2O , NH_3 and THF chelation to the stabilization of complex I-8 (^tBu -PNP-Ir); (b): The effect of H_2O , NH_3 and THF to the stabilization of complex I-8 (^tBu -PNP-Fe), (c): The effect of H_2O , NH_3 and THF to the stabilization of complex I-8 (^tBu -PNP-Ru), Table S4: Testing the stability of H_2O chelation to the Ir complexes, Table S5: (a): Energies of each compounds for the simplified model (H_2P -) with NH_3 chelation. G_{corr} = Thermal correction to Gibbs Free Energy; E = Absolute single-point energies; G = Gibbs free energies; (b): Energies of each compounds for the complete model ($^t\text{Bu}_2\text{P}$ -) with H_2O , NH_3 and THF chelation. G_{corr} = Thermal correction to Gibbs Free Energy; E = Absolute single-point energies; G = Gibbs free energies; (c): Energies of each compounds for the complete model (Ada_2P -) with H_2O , NH_3 and THF chelation. G_{corr} = Thermal correction to Gibbs Free Energy; E = Absolute single-point energies; G = Gibbs free energies. Table S6: Cartesian coordinates for the molecules involved in Pathway I-B and Pathway 2a.

Author Contributions: Conceptualization, Y.L. and C.-W.T.; methodology, Y.L., C.-W.T. and E.M.H.C.; software, Y.L.; validation, Y.L., C.-W.T. and E.M.H.C.; formal analysis, Y.L. and C.-W.T.; investigation, X.-Y.L. and C.L.; resources, E.Y.C.W. and D.C.K.H.; data curation, Y.L.; writing—original draft, C.-W.T. and E.M.H.C.; writing—review and editing, Y.L. and C.-W.T.; supervision, C.-W.T. and C.L.; project administration, C.-W.T. and C.L.; funding acquisition, C.-W.T. and E.Y.C.W. All authors have read and agreed to the published version of the manuscript.

Funding: This research was fully funded by Hong Kong University Grants Committee—Institutional Development Scheme (IDS) Collaborative Research Grant, grant number UGC/IDS(C)14/B(E)01/19.

Acknowledgments: We thank Bin Wang for his helpful discussion.

Conflicts of Interest: The authors declare no conflict of interest.

References

1. Energy Department Announces \$15.8 Million Investment for Innovation in Hydrogen and Fuel Cell Technologies; Office of Energy Efficiency & Renewable Energy, Department of Energy: Washington, DC, USA, 2017.
2. Marco-Lozar, J.; Juan-Juan, J.; Suárez-García, F.; Cazorla-Amorós, D.; Linares-Solano, A. MOF-5, and activated carbons as adsorbents for gas storage. *Int. J. Hydrogen Energy* **2012**, *37*, 2370–2381. [[CrossRef](#)]
3. Luo, W.; Campbell, P.G.; Zakharov, L.N.; Liu, S.-Y. A Single-component liquid-phase hydrogen storage material. *J. Am. Chem. Soc.* **2011**, *133*, 19326–19329. [[CrossRef](#)] [[PubMed](#)]
4. Bogdanović, B.; Schwickardi, M. Ti-doped alkali metal aluminium hydrides as potential novel reversible hydrogen storage materials. *J. Alloys Compd.* **1997**, *253*, 1–9. [[CrossRef](#)]
5. Demirci, U.B. Ammonia borane, a material with exceptional properties for chemical hydrogen storage. *Int. J. Hydrogen Energy* **2017**, *42*, 9978–10013. [[CrossRef](#)]
6. Demirci, U.B.; Miele, P. Sodium borohydride versus ammonia borane, in hydrogen storage and direct fuel cell applications. *Energy Environ. Sci.* **2009**, *2*, 627. [[CrossRef](#)]
7. Rossin, A.; Peruzzini, M. Ammonia–borane and amine–borane dehydrogenation mediated by complex metal hydrides. *Chem. Rev.* **2016**, *116*, 8848–8872. [[CrossRef](#)]
8. Moury, R.; Demirci, U.B. Hydrazine borane and hydrazinoboranes as chemical hydrogen storage materials. *Energies* **2015**, *8*, 3118–3141. [[CrossRef](#)]
9. Zhao, Q.; Li, J.; Hamilton, E.J.; Chen, X. The continuing story of the diammoniate of diborane. *J. Organomet. Chem.* **2015**, *798*, 24–29. [[CrossRef](#)]
10. Bhunya, S.; Malakar, T.; Ganguly, G.; Paul, A. Combining protons and hydrides by homogeneous catalysis for controlling the release of hydrogen from ammonia–borane: Present status and challenges. *ACS Catal.* **2016**, *6*, 7907–7934. [[CrossRef](#)]
11. Staubitz, A.; Robertson, A.; Manners, I. Ammonia-borane and related compounds as dihydrogen sources. *Chem. Rev.* **2010**, *110*, 4079–4124. [[CrossRef](#)]
12. Summerscales, O.T.; Gordon, J.C. Regeneration of ammonia borane from spent fuel materials. *Dalton Trans.* **2013**, *42*, 10075. [[CrossRef](#)] [[PubMed](#)]
13. Bandaru, S.; English, N.J.; Phillips, A.D.; MacElroy, J.M.D. Exploring promising catalysts for chemical hydrogen storage in ammonia borane: A Density functional theory study. *Catalysts* **2017**, *7*, 140. [[CrossRef](#)]
14. Denney, M.C.; Pons, V.; Hebden, T.J.; Heinekey, D.M.; Goldberg, K.I. Efficient catalysis of ammonia borane dehydrogenation. *J. Am. Chem. Soc.* **2006**, *128*, 12048–12049. [[CrossRef](#)] [[PubMed](#)]
15. Graham, T.W.; Tsang, C.-W.; Chen, X.; Guo, R.; Jia, W.; Lu, S.-M.; Sui-Seng, C.; Ewart, C.B.; Lough, A.; Amoroso, D.; et al. Catalytic solvolysis of ammonia borane. *Angew. Chem. Int. Ed.* **2010**, *49*, 8708–8711. [[CrossRef](#)] [[PubMed](#)]
16. Stevens, C.J.; Dallanegra, R.; Chaplin, A.B.; Weller, A.S.; MacGregor, S.A.; Ward, B.; McKay, D.; Alcaraz, G.; Sabo-Etienne, S. Ir(PCy₃)₂(H)₂(H₂B-NMe₂)⁺ as a latent source of aminoborane: Probing the role of metal in the dehydrocoupling of H₃B-NMe₂H and retrodimerisation of [H₂BNMe₂]₂. *Chem. A Eur. J.* **2011**, *17*, 3011–3020. [[CrossRef](#)]
17. Johnson, H.C.; Robertson, A.; Chaplin, A.B.; Sewell, L.J.; Thompson, A.L.; Haddow, M.; Manners, I.; Weller, A.S. Catching the first oligomerization event in the catalytic formation of polyaminoboranes: H₃B-NMeHBH₂-NMeH₂ Bound to iridium. *J. Am. Chem. Soc.* **2011**, *133*, 11076–11079. [[CrossRef](#)]
18. Fortman, G.C.; Slawin, A.M.Z.; Nolan, S.P. Highly Active iridium (III)–NHC system for the catalytic B–N bond activation and subsequent solvolysis of ammonia–borane. *Organometallics* **2011**, *30*, 5487–5492. [[CrossRef](#)]
19. Ai, D.-X.; Qi, Z.-H.; Ruan, G.-Y.; Zhang, Y.; Liu, W.; Wang, Y. DFT studies of dehydrogenation of ammonia–borane catalyzed by Ir(ItBu)²⁺: A proton transfer mechanism. *Comput. Theor. Chem.* **2014**, *1048*, 1–6. [[CrossRef](#)]
20. Tang, C.Y.C.; Phillips, N.; Kelly, M.; Aldridge, S. Hydrogen shuttling: Synthesis and reactivity of a 14-electron iridium complex featuring a bis(alkyl) tethered N-heterocyclic carbene ligand. *Chem. Commun.* **2012**, *48*, 11999. [[CrossRef](#)]

21. Wang, W.-H.; Tang, H.-P.; Lu, W.-D.; Li, Y.; Bao, M.; Himeda, Y. Mechanistic insights into the catalytic hydrolysis of ammonia borane with proton-responsive iridium complexes: An experimental and theoretical study. *ChemCatChem* **2017**, *9*, 3191–3196. [CrossRef]
22. Rossin, A.; Caporali, M.; Gonsalvi, L.; Guerri, A.; Lledós, A.; Peruzzini, M.; Zanolini, F. Selective B-H versus N-H Bond activation in ammonia borane by Ir(dppm)₂OTf. *Eur. J. Inorg. Chem.* **2009**, *2009*, 3055–3059. [CrossRef]
23. von Colbe, J.B.; Ares, J.-R.; Barale, J.; Baricco, M.; Buckley, C.; Capurso, G.; Gallandat, N.; Grant, D.M.; Guzik, M.N.; Jacob, I.; et al. Application of hydrides in hydrogen storage and compression: Achievements, outlook and perspectives. *Int. J. Hydrogen Energy* **2019**, *44*, 7780–7808. [CrossRef]
24. Cobalt prices continue to climb due to market uncertainty. *Met. Powder Rep.* **1999**, *54*, 4. [CrossRef]
25. Iridium Prices. Available online: <https://www.umicore.com/en/about/elements/iridium/> (accessed on 29 May 2020).
26. Lin, T.-P.; Peters, J.C. Boryl–metal bonds facilitate cobalt/nickel-catalyzed olefin hydrogenation. *J. Am. Chem. Soc.* **2014**, *136*, 13672–13683. [CrossRef] [PubMed]
27. Ge, H.; Jing, Y.; Yang, X. Computational design of cobalt catalysts for hydrogenation of carbon dioxide and dehydrogenation of formic acid. *Inorg. Chem.* **2016**, *55*, 12179–12184. [CrossRef] [PubMed]
28. Fu, S.; Chen, N.-Y.; Liu, X.; Shao, Z.; Luo, S.-P.; Liu, Q. Ligand-controlled cobalt-catalyzed transfer hydrogenation of alkynes: Stereodivergent synthesis of Z- and E-alkenes. *J. Am. Chem. Soc.* **2016**, *138*, 8588–8594. [CrossRef]
29. Alpaydin, C.Y.; Gülbay, S.K.; Colpan, C.O. A review on the catalysts used for hydrogen production from ammonia borane. *Int. J. Hydrogen Energy* **2020**, *45*, 3414–3434. [CrossRef]
30. Nuss, P.; Eckelman, M.J. Life Cycle assessment of metals: A scientific synthesis. *PLoS ONE* **2014**, *9*, e101298. [CrossRef]
31. Ghatak, K.; Vanka, K. A computational investigation of the role of the iridium dihydrogen pincer complex in the formation of the cyclic pentamer (NH₂BH₂)₅. *Comput. Theor. Chem.* **2012**, *992*, 18–29. [CrossRef]
32. Paul, A.; Musgrave, C.B. Catalyzed dehydrogenation of ammonia–borane by iridium dihydrogen pincer complex differs from ethane dehydrogenation. *Angew. Chem. Int. Ed.* **2007**, *46*, 8153–8156. [CrossRef]
33. Ciganda, R.; Garralda, M.A.; Ibarlucea, L.; Pinilla, E.; Torres, M.R. A hydrido-irida-β-diketone as an efficient and robust homogeneous catalyst for the hydrolysis of ammonia–borane or amine–borane adducts in air to produce hydrogen. *Dalton Trans.* **2010**, *39*, 7226. [CrossRef] [PubMed]
34. Garralda, M.A.; Mendicute-Fierro, C.; Rodríguez-Diéguez, A.; Seco, J.M.; Ubide, C.; Zumeta, I. Efficient hydrido-irida-β-diketone-catalyzed hydrolysis of ammonia- or amine-boranes for hydrogen generation in air. *Dalton Trans.* **2013**, *42*, 11652. [CrossRef] [PubMed]
35. Nelson, D.; Truscott, B.; Egbert, J.D.; Nolan, S.P. Exploring the limits of catalytic ammonia–borane dehydrogenation using a bis (N-heterocyclic carbene) iridium (III) complex. *Organometallics* **2013**, *32*, 3769–3772. [CrossRef]
36. Umegaki, T.; Yan, J.-M.; Zhang, X.; Shioyama, H.; Kuriyama, N.; Xu, Q. Preparation, and catalysis of poly(N-vinyl-2-pyrrolidone) (PVP) stabilized nickel catalyst for hydrolytic dehydrogenation of ammonia borane. *Int. J. Hydrogen Energy* **2009**, *34*, 3816–3822. [CrossRef]
37. Abdur-Rashid, K.; Graham, T.; Tsang, C.-W.; Chen, X.; Guo, R.; Jia, W.; Amoroso, D.; Sui-Seng, C. The Generation of Hydrogen from Ammonia Borane through Catalytic Hydrolysis. International Patent WO2008141439A1, 2008.
38. Abdur-Rashid, K.; Graham, T.; Tsang, C.-W.; Chen, X.; Guo, R.; Jia, W. Method to Produce Hydrogen from the Dehydrocoupling of Amine Boranes. US Patent US9115249B2, 2015.
39. Freixa, Z.; Garralda, M.A. Insights into the use of [Ru(p-Cym)(bipy)Cl]Cl as precatalyst for solvolytic dehydrogenation of ammonia-borane. *Inorganica Chim. Acta* **2015**, *431*, 184–189. [CrossRef]
40. Frisch, M.J.; Trucks, G.W.; Schlegel, H.B.; Scuseria, G.E.; Robb, M.A.; Cheeseman, J.R.; Scalmani, G.; Barone, V.; Mennucci, B.; Petersson, V.; et al. *Gaussian 09 (Revision D.01)*; Gaussian, Inc.: Wallingford, CT, USA, 2013.
41. Lee, C.; Yang, W.; Parr, R.G. Development of the Colle-Salvetti correlation-energy formula into a functional of the electron density. *Phys. Rev. B* **1988**, *37*, 785–789. [CrossRef]
42. Becke, A.D. Density-functional thermochemistry. III. The role of exact exchange. *J. Chem. Phys.* **1993**, *98*, 5648–5652. [CrossRef]

43. Zhao, Y.; Truhlar, D.G. The M06 suite of density functionals for main group thermochemistry, thermochemical kinetics, noncovalent interactions, excited states, and transition elements: Two new functionals and systematic testing of four M06-class functionals and 12 other functionals. *Theor. Chem. Accounts* **2007**, *120*, 215–241. [[CrossRef](#)]
44. Dunning, T.H., Jr.; Hay, P.J. *Modern Theoretical Chemistry*; Schaefer, H.F., Ed.; Plenum Press: New York, NY, USA, 1977; pp. 1–28.
45. Fukui, K.; Fujimoto, H. A formulation of the reaction coordinate. *Quant. Chem.* **1997**, *7*, 371–373. [[CrossRef](#)]
46. Fukui, K. The path of chemical reactions—The IRC approach. *Acc. Chem. Res.* **1981**, *14*, 363–368. [[CrossRef](#)]
47. Aleksandr, V.M.; Christopher, J.C.; Donald, G.T. Universal solvation model based on solute electron density and on a continuum model of the solvent defined by the bulk dielectric constant and atomic surface tensions. *J. Phys. Chem. B* **2009**, *113*, 6378–6396.
48. Tamura, H.; Yamazaki, H.; Sato, H.; Sakaki, S. Iridium-catalyzed borylation of benzene with diboron. Theoretical elucidation of catalytic cycle including unusual iridium(V) intermediate. *J. Am. Chem. Soc.* **2003**, *125*, 16114–16126. [[CrossRef](#)] [[PubMed](#)]
49. Li, Y.; Hou, C.; Jiang, J.; Zhang, Z.; Zhao, C.; Page, A.J.; Ke, Z. General H₂ activation modes for Lewis acid–transition metal bifunctional catalysts. *ACS Catal.* **2016**, *6*, 1655–1662. [[CrossRef](#)]
50. Wenz, K.M.; Liu, P.; Houk, K.N. Intramolecular C–H Activation reactions of ru (NHC) complexes combined with H₂ transfer to alkenes: A theoretical elucidation of mechanisms and effects of ligands on reactivities. *Organometallics* **2017**, *36*, 3613–3623. [[CrossRef](#)]
51. Wang, X.; Li, Y.; Knecht, T.; Daniliuc, C.; Houk, K.N.; Glorius, F. Unprecedented dearomatized spirocyclopropane in a sequential rhodium (III)-catalyzed C–H activation and rearrangement reaction. *Angew. Chem. Int. Ed.* **2018**, *57*, 5520–5524. [[CrossRef](#)] [[PubMed](#)]
52. Chen, S.; Zheng, Y.; Cui, T.; Meggers, E.; Houk, K.N. Arylketone π -conjugation controls enantioselectivity in asymmetric alkynylations catalyzed by centrochiral ruthenium complexes. *J. Am. Chem. Soc.* **2018**, *140*, 5146–5152. [[CrossRef](#)] [[PubMed](#)]
53. Zhou, Z.; Chen, S.; Hong, Y.; Winterling, E.; Tan, Y.; Hemming, M.; Harms, K.; Houk, K.N.; Meggers, E. Non-C₂-symmetric chiral-at-ruthenium catalyst for highly efficient enantioselective intramolecular C(sp³)-H amidation. *J. Am. Chem. Soc.* **2019**, *141*, 19048–19057. [[CrossRef](#)] [[PubMed](#)]
54. Bai, H.; Zhang, H.; Zhang, X.; Wang, L.; Li, S.-J.; Wei, D.; Zhu, Y.; Zhang, W. Unravelling the origins of hydroboration chemoselectivity inversion using an N,O-chelated Ir (I) complex: A computational study. *J. Org. Chem.* **2019**, *84*, 6709–6718. [[CrossRef](#)]



© 2020 by the authors. Licensee MDPI, Basel, Switzerland. This article is an open access article distributed under the terms and conditions of the Creative Commons Attribution (CC BY) license (<http://creativecommons.org/licenses/by/4.0/>).